

1 **Autonomic modulation of the electrical substrate in mice**
2 **haploinsufficient for cardiac sodium channels: a model of**
3 **the Brugada syndrome.**

4
5
6 Malcolm Finlay¹, Justine Bhar-Amato², Keat-Eng Ng¹, Diogo Santos², Michele Orini², Vishal
7 Vyas¹, Peter Taggart², Andrew A. Grace³, Christopher L.-H. Huang⁴, Pier D. Lambiase² &
8 Andrew Tinker¹

9
10 ¹William Harvey Research Institute, Barts and the London School of Medicine and Dentistry,
11 Queen Mary University of London, London, UK

12 ²Institute of Cardiovascular Science, University College London, London, UK

13 ³Department of Biochemistry, University of Cambridge, Cambridge, United Kingdom

14 ⁴Department of Physiology, Development and Neuroscience, University of Cambridge,
15 Cambridge, United Kingdom

16
17 Running Title: Autonomic modulation of cardiac conduction velocity

18
19 Total Word Count: 5318

20
21 Address for Correspondence: Professor Andrew Tinker, William Harvey Heart Centre,
22 Barts & The London School of Medicine & Dentistry, Charterhouse Square, London EC1M
23 6BQ. Tel: 020 7882 5783, E-mail: a.tinker@qmul.ac.uk

25

Abstract

26

27

28

29

30

31

32

33

34

35

36

37

38

39

40

41

42

43

44

A murine line haploinsufficient in the cardiac sodium channel has been used to model human Brugada syndrome: a disease causing sudden cardiac death due to lethal ventricular arrhythmias. We explored the effects of cholinergic tone on electrophysiological parameters in wild type and genetically modified, heterozygous, *Scn5a*^{+/-} knockout mice. *Scn5a*^{+/-} ventricular slices showed longer refractory periods than wild-type both at baseline and during isoprenaline challenge. *Scn5a*^{+/-} hearts also showed lower conduction velocities and increased mean increase in delay than did littermate controls at baseline and blunted responses to isoprenaline challenge. Carbachol exerted limited effects but reversed the effects of isoprenaline with co-application. *Scn5a*^{+/-} mice showed a reduction in conduction reserve in that isoprenaline no longer increased conduction velocity and this was not antagonised by muscarinic agonists.

Key Words: autonomic nervous system, conduction, *SCN5A* haploinsufficiency, Brugada syndrome

Abbreviations: MEA – multielectrode array, VERP – ventricular refractory period, *Scn5a*^{+/-} – cardiac sodium channel (*Scn5a*) haploinsufficient mouse

Introduction

45

46

47 Brugada Syndrome is recognised by a triad of right bundle branch block, coved ST
48 elevation in the right precordial leads and lethal ventricular arrhythmias (6; 25). It may be
49 responsible for up to a fifth of cases of sudden cardiac death in the young (25). Where a
50 mutation is identified this most commonly occurs in the main cardiac sodium channel
51 isoform, SCN5A (4) though in many patients no obvious mutations are found. The main
52 pathophysiological feature is the presence of significant cardiac conduction delays
53 particularly in the right ventricular outflow tract and these contribute to the ECG pattern and
54 arrhythmic predisposition (15). Furthermore, it is well known that sodium channel density is
55 an important determinant of conduction velocity in the heart (14).

56 An interesting feature of Brugada Syndrome is that ventricular arrhythmia occurs at
57 night when the patient is sleeping and this can be accompanied by accentuation of the
58 characteristic ECG pattern (21; 23). The autonomic nervous system is well known to
59 modulate ventricular excitability; however in many other channelopathies it is exercise or
60 stress that precipitates ventricular tachycardia and/or fibrillation and thus this observation is
61 intriguing (9). During rest, vagal activity is predominant in contrast to the situation in
62 exercise where vagal activity is reduced and sympathetic drive predominates though the
63 detailed picture may be more complex than this standard interpretation (18). In this study, we
64 explore this question in a model of Brugada Syndrome namely the SCN5A- haploinsufficient
65 mouse (*Scn5a+/-*). This model recapitulates a number of the features of Brugada syndrome
66 seen in patients (11; 12; 19; 24) and provides a route to exploring the autonomic modulation
67 of the electrophysiological substrate.

68

Methods

69

70

71 *Murine breeding and genotyping*

72 Mice were maintained in an animal core facility under UK Home Office guidelines
73 relating to animal welfare. All mice were kept in individually ventilated, pathogen-free,
74 temperature controlled cages (21-23°C) with 12-hour day/night light cycles. Animals had free
75 access to standard rodent chow and water. Mice of both sexes were studied between 12 and
76 24 weeks of age under standardized conditions for tissue slice analysis. Whole heart studies
77 were performed at between 9 months and 1 year of age in mice of both sexes. The generation
78 of the *Scn5a*^{+/-} heterozygotic mice has been previously described (24). Genotyping was
79 performed at 6 weeks of age. Littermate controls were used throughout, and experiments and
80 analysis were performed blinded to genotype (MF, VV). The work was carried out under UK
81 Home Office project licences PPL-6732 and PPL-7665.

82

83 *Cardiac Excision*

84 Mice were euthanized by cervical dislocation. The thorax was immediately dissected
85 and the heart exposed. Cardioplegia was induced by applying 10 ml of ice-cold, oxygenated
86 (bubbled with 95% O₂; 5% CO₂) Ca²⁺-free Krebs solution (119 mM NaCl, 4 mM KCl, 1 mM
87 MgCl₂, 1.2 mM KH₂PO₄, 25 mM NaHCO₃, 10 mM glucose, 2 mM Na pyruvate, pH 7.4)
88 directly onto the epicardial surface. The heart and great vessels were removed within 20 sec
89 and placed into a dissection dish containing oxygenated ice-cold Ca²⁺-free Krebs solution. A
90 23 gauge cannula was inserted into the aorta and secured under light microscopy. For tissue
91 slicing, cold retrograde perfusion was commenced with oxygenated, ice-cold, Ca²⁺ free Krebs
92 solution at a flow rate of 16.5 ml/min. Whole-heart recording perfusion used oxygenated

93 Krebs solution (containing 1.4 mM Ca^{2+}) at room temperature. The time taken from cervical
94 dislocation to establishment of Langendorff perfusion was less than 3 min.

95

96 *Preparation of cardiac tissue slices*

97 Following perfusion for 2 min, the perfusate was altered to an ice-cold oxygenated
98 Ca^{2+} -free Krebs solution containing high K^+ (20 mM KCl) and blebbistatin (20 μM ;
99 Cambridge Bioscience, Cambs, UK) for 3 minutes. The hearts were then removed from the
100 Langendorff perfusion rig and placed again in a dissection dish containing cold perfusate.
101 Ventricular tissue was dissected from atrial tissue under light microscopy. The dissected
102 ventricles were then embedded in low-melt agarose (4% low-melting point agarose in Ca^{2+} -
103 free Krebs solution), and then rapidly chilled on ice. The agarose block was orientated and
104 fixed onto a magnetic stage using cyanoacrylate glue and placed in the cutting chamber of a
105 Vibratome (Campden Instruments, London, UK). This chamber was maintained at 4°C using
106 external ice. It was filled with cold, modified oxygenated Krebs solution (containing 0.6 mM
107 Ca^{2+} , 10 mM K^+). Tissue sections were obtained from apex to base at an interval thickness of
108 200 μm . The vibrating PTFE-coated steel blade (Wilkinson Sword, Bucks, UK) was
109 advanced at <200 $\mu\text{m}/\text{sec}$. The x-axis vibration was applied at an amplitude of 2 mm and
110 frequency of 80 Hz. The z-axis deviation was calibrated prior to every use to be < 1 μm . The
111 cut sections were immediately placed in oxygenated low- Ca^{2+} Krebs solution (4 mM KCl, 0.6
112 mM Ca^{2+}) containing 10 mM blebbistatin maintained at room temperature. After 25 minutes,
113 the samples were transferred to standard oxygenated Krebs solution (4 mM KCl, 1.1 mM
114 Ca^{2+}) and kept at room temperature until electrophysiological studies were performed.

115

116 *Cardiac slice electrophysiological (EP) studies*

117 Stimulation was generated by a stimulus isolation unit (DS-2A, Warner Instruments,
118 MA, USA) with signal timing driven by an Arduino Uno microcontroller (Arduino, It).
119 Stimulation was applied using a silver chloride bipolar electrode. The sections were placed in
120 the recording chamber and carefully positioned manually so that left ventricular tissue
121 overlaid the measurement electrodes. A 1 cm diameter metal ring with an overlying nylon
122 mesh (Harp-slice grid, Micro Control Instruments, East Sussex, UK) was used to hold the
123 tissue flat in place on the electrode grid and ensured adequate tissue electrode contact. The
124 recording chamber was mounted in the headstage and perfusion commenced at 2 ml/min.
125 Tissue was allowed to settle to a steady state over 1 min before electrode placement. The
126 bipolar stimulating electrode was carefully lowered to just contact the tissue slice on the left
127 ventricular tissue, but not to move the slice on the array. Stimulation was started at a
128 frequency of 5 Hz using a monophasic 1 ms duration pulse, for real-time recording of
129 electrical activity. The stimulus voltage was increased until electrical capture was achieved.
130 The stimulus voltage was then reduced until electrical capture was lost: the lowest voltage
131 stimulus that could reliably achieve capture was then taken as the stimulus threshold. Cardiac
132 signals were recorded at a sampling frequency of 10 kHz. A simulation protocol was
133 performed with steady state pacing at an interstimulus interval of 200 ms, with stimulation
134 during recording applied at an amplitude of twice threshold. Around 30 sec of pacing activity
135 were recorded for each state for each slice. Perfusate solution containing drugs was washed in
136 over 30 seconds at 20 ml/min. Slices were then stimulated at 5 Hz for 2 min before threshold
137 was determined and recording commenced.

138

139 *Ex-vivo whole heart recordings*

140 For whole heart recordings, hearts were retrogradely perfused at 16.5 ml/min with
141 normal oxygenated Krebs solution (Ca^{2+} 1.4 mM). A unipolar silver chloride stimulation

142 electrode and flexible 32-pole multi-electrode array (MEA) (FlexMEA, Multielectrode
143 Systems) were placed on the ventricular epicardium and an S₁S₂ decremental stimulation
144 protocol was performed to determine the ventricular effective refractory period (VERP).
145 Stimulation was performed with a biphasic pulse of amplitude 2 V and duration 0.5 ms, with
146 S₁S₂ intervals reduced from 150 ms by decrements of 5 ms to 100 ms and thereafter by
147 decrements of 2 ms until tissue refractoriness was reached. Arrhythmogenicity was further
148 tested for by applying stimulating trains of 100 beats at coupling intervals progressively
149 reduced from 100 ms. Ventricular tachycardia was defined as a ventricular arrhythmia
150 persisting more than 2 sec.

151

152 *Analysis of electrograms*

153 All analysis of murine electrophysiology was performed using custom software
154 running in Matlab, v2014b (The Mathworks Inc., MA, USA). The time point of local
155 activation was taken at the steepest negative gradient of the unipolar electrogram. Conduction
156 velocities were determined using a gradient method, with conduction velocity defined as the
157 inverse of the gradient in activation times across the array (Figure 1A-C). Electrodes with
158 significant noise were excluded, and all electrograms and time points were checked manually.
159 Mean increase in delay (MID), a well-validated measure of inducibility of conduction delay,
160 was calculated by determining the area under the conduction-delay curve (15) and according
161 to the equation

162

$$MID = \frac{\left(\int_{minS2 CI}^{S1 CI} (Activation Time - Activation Time at S1CI) \right)}{S1 CI - minS2 CI}$$

163

164

165 Where MID is Mean Increase in Delay, S1 CI is the coupling interval of steady state pacing
166 (S1) and minS2 CI is the minimum coupling interval above ERP. The integral was calculated
167 using the trapz function in Matlab.

168 The mean timing of the activation time of all recording electrodes was used for each
169 measurement of conduction delay, and the MID defined as the unit increase in conduction
170 delay per unit reduction in S_1S_2 coupling interval (ms/ms). Stimulation protocols were
171 performed in normal Krebs's solution, in baseline (control) conditions or with isoprenaline
172 100 nM and/or carbachol 10 μ M.

173

174 *Immunofluorescence of cardiac sections*

175 Mouse hearts were rinsed in PBS and cut longitudinally with a blade and tissue
176 holder. The hearts were fixed in 10% formalin (Sigma) for at least 24 hours followed by two
177 PBS washes and stored in 70% ethanol before paraffin embedding. Paraffin-embedded hearts
178 were cut to 5 μ m thick sections and mounted on Superfrost plus microscope slides. Sections
179 were then deparaffinized with xylene and rehydrated with 4 ethanol washes (from 100%-
180 50%) before heat-mediated antigen retrieval with citrate buffer (pH 6.0). Following antigen
181 retrieval, sections were washed several times in PBS, permeabilized with 0.1% Triton X-100
182 for 15 minutes and blocked with 5% goat serum in PBS for 1 hour at room temperature.
183 Sections were then incubated with primary antibodies with 1% goat serum overnight at 4°C:
184 Mouse monoclonal Cx43 clone 4E6.2 (Millipore MAB3067) and rabbit polyclonal N
185 cadherin antibody (Santa Cruz SC-7939). The sections were incubated with fluorescently
186 labelled secondary antibodies Alexa Fluor goat anti-mouse 488 and goat anti-rabbit 555
187 secondary antibodies (Invitrogen, UK) for 1 hour at room temperature in the dark. Sections
188 were washed several times with PBS and co-stained with DAPI (nuclear stain) and stored in
189 the dark until further analysis. The samples were analyzed using confocal microscopy (LSM

190 510, Carl Zeiss with DAPI: Excitation 405 nm, Emission LP420, FITC: Excitation 488
191 nm, Emission BP 505-550 and Cy3: Excitation 543 nm, Emission LP 560. Images were
192 acquired sequentially. Quantitative analysis of the images was performed using ImageJ.
193 Thresholding was applied to the images and they were then converted to binary files. The
194 Cx43 stained image was subtracted by the N-cadherin stained image and represented “Cx43
195 not located at the intercalated disk”.

196

197 *Statistical analysis*

198 All statistical analysis was performed using R software (The Comprehensive R
199 Archive Network (CRAN)). Continuous parametric data are presented as means \pm standard
200 deviations (SD) or, in the case of significance derived from regression models, mean with
201 [95% confidence interval], unless otherwise specified. Comparisons in which a single
202 measurement was taken for each subject, e.g. ventricular effective refractory period (VERP),
203 dispersion of repolarisation time, were made using Student’s t-test with post-hoc correction
204 for multiple comparisons. Continuous parametric data derived from electrogram data were
205 modelled using mixed-effects linear regression (software: Linear and Nonlinear Mixed
206 Effects (NLME) package running in R version 2.14) and statistical significance was inferred
207 from the model. Quartile regression with bootstrapping (Quantile Regression Description
208 Estimation and inference (QUANTREG) package) was used to compare non-parametric
209 continuous data. Statistical significance is indicated by * $p < 0.05$, ** $p < 0.01$ and *** $p < 0.001$.

210

211

Results

212

213

214 There are conflicting reports of the effects of autonomic modulation on
215 electrophysiological parameters in ventricular tissue such as conduction velocity (7). We
216 accordingly investigated the effects of autonomic challenge on indices representing activation
217 and recovery in littermate normal murine hearts and *Scn5a*-haploinsufficient heterozygous
218 (*Scn5a*^{+/-}) mice. We used two approaches to examine tissue level electrophysiology: tissue
219 slices from juvenile animals (aged 2-3 months) placed on a MEA system, and *ex-vivo*
220 Langendorff perfused hearts from mature animals (aged 9 months to a year) studied using an
221 externally applied electrode array. Previous studies in older Langendorff perfused hearts had
222 associated arrhythmic phenotypes with the *Scn5a*^{+/-} genotype but we were unable to obtain
223 viable tissue slices from older animals for multi-electrode array studies. We applied
224 isoprenaline as a β -adrenoreceptor activator to mimic sympathetic activation and the
225 muscarinic receptor agonist carbachol, to approximate vagal activation.

226 Ventricular slices obtained from juvenile *Scn5a*^{+/-} mice required higher stimulus
227 voltages than did wildtype (4.0 ± 0.7 vs 2.7 ± 0.4 V at baseline, **) for consistent capture,
228 both before, and following all the different pharmacological manipulations. Untreated slices
229 from *Scn5a*^{+/-} hearts showed a trend towards lower conduction velocities than WT hearts
230 (0.31 ± 0.04 vs 0.40 ± 0.7 m/s), but this was not statistically significant. Isoprenaline (100
231 nM) challenge increased conduction velocity in slices from wildtype (0.58 ± 0.11 m/s) but
232 not in *Scn5a*^{+/-} heart slices (0.34 ± 0.05 m/s) *. The increase in conduction velocity was
233 reversed with carbachol co-application (Figure 2). Tissue slices from *Scn5a*^{+/-} hearts showed
234 consistently longer effective refractory periods both before (means \pm SEM: *Scn5a*^{+/-} 79 ± 4
235 vs WT 63 ± 4 ms, ***) and during isoprenaline challenge (73 ± 7 vs 52 ± 7 ms). Carbachol

236 markedly shortened the VERP in slices from WT but not *Scn5a*^{+/-} hearts (*Scn5a*^{+/-}: 76±7
237 ms, WT: 41±5 ms **).

238 In Langendorff-perfused isolated hearts, S₁S₂ decremental protocols were attempted
239 before pharmacological challenge, and in the presence of isoprenaline 100 nM, and/or
240 carbachol 10 μM. However, pacing capture became inconsistent during carbachol
241 administration in 6 out of 8 *Scn5a*^{+/-} hearts, despite attempts at increasing stimulation
242 amplitude. Data from Langendorff-perfused *Scn5a*^{+/-} hearts were therefore formally
243 analysed for isoprenaline effects only (n=11) and were compared to littermate WT hearts
244 (n=10). Washout (5 mins) was performed between drug challenges. *Scn5a*^{+/-} hearts showed
245 blunted responses to isoprenaline, mimicking the data from the cardiac tissue slice
246 preparations (Figure 3). Notably, a 16% increase in conduction velocity observed in WT
247 hearts in response to isoprenaline was again blunted in *Scn5a*^{+/-} hearts (normalised
248 conduction velocity control vs *Scn5a*^{-/-} response to isoprenaline **), which exhibited a
249 marginal decrease in conduction velocity. No consistent changes in electrophysiological
250 parameters were observed during carbachol administration in the WT group.

251 Induced conduction delay in response to premature extrastimuli was also investigated.
252 Mean increase in delay was almost double in *Scn5a*^{+/-} hearts compared to WT controls
253 (***). Controls and *Scn5a*^{+/-} murine hearts studied through these procedures did not show
254 differences in arrhythmia inducibility under control conditions, or isoprenaline 100 nM or
255 carbachol 10 μM challenge (arrhythmic phenomena shown in 1/7 hearts in both drug
256 challenges, with no sustained arrhythmias in either *Scn5a*^{-/+} or controls). Little consistent
257 change in VERP with drug challenge was observed in whole heart preparations (Figure 3C).

258 Finally we investigated a possible relationship between haploinsufficiency of *Scn5a*
259 and the localization and expression of Cx43 in the juvenile animals. The expression of Cx43
260 was not grossly changed but there was an impression of localisation away from the

261 intercalated disc (marked by N-Cadherin staining) and into the cytosol (Figure 4). We
262 confirmed this by quantifying the redistribution as detailed in the Methods. We expressed the
263 localisation as a ratio of the amount of Cx43 not at the intercalated divided by the total
264 expression of Cx43. In wildtype mice this number was $53.7 \pm 3.9\%$ and in *Scn5a*^{+/-} mice
265 $71.6\% \pm 2.7\%$ (n=5 both groups, P<0.01).
266

Discussion

267
268

269 In this study we have investigated the tissue level electrophysiological properties of
270 ventricles from *Scn5a* haploinsufficient mice and compared these to littermate controls. Our
271 main finding is that there is an impairment of the response of conduction velocity to
272 autonomic challenge in *Scn5a*^{+/-} mice. In hearts from control mice, isoproterenol increased
273 conduction velocity and decreased mean propagation delays. *Scn5a*^{+/-} hearts demonstrated a
274 reduced response of conduction velocity with increased mean propagation delays in response
275 to isoprenaline. This effect was reversed by further challenge with carbachol, a muscarinic
276 agonist although carbachol alone did not have prominent effects. This is consistent with
277 previous reports that sympathetic activation increases conduction velocity in normal hearts (2;
278 7). In heart slice preparations in juvenile animals, ERP was prolonged in *Scn5a*^{+/-} hearts
279 whilst in older animals there was no significant difference when studied in Langendorff
280 perfused intact hearts.

281 The findings in murine hearts may correlate with previous reports that β -
282 adrenoreceptor activation increases sodium currents and therefore action potential conduction
283 velocity through a protein kinase A dependent mechanism (20); reduced effects of
284 isoprenaline could then be associated with the Na⁺ channel haploinsufficiency in *Scn5a*^{+/-}
285 hearts. There is also the possibility that signalling pathways downstream of the β -adrenergic
286 signalling pathway may also modulate gap junction density at the intercalated disc (7; 16).
287 We also saw a potential mislocalization of Cx43 away from the intercalated disk in sodium
288 channel haploinsufficient mice and this may contribute to the conduction slowing. It is
289 plausible that some form of interaction with scaffolding or other proteins may be responsible
290 for maintaining stoichiometry of Cx43 and *Scn5a* at the intercalated disk. A number of
291 interacting sodium channel proteins are known and Cx43 can influence the trafficking of
292 *Scn5a* (1; 27). This is a topic for investigation in future studies. We did not see prominent

293 responses to carbachol in tissue level electrophysiological parameters after washout of
294 isoprenaline. However, combined application of both isoprenaline and carbachol in wildtype
295 tissue slices reversed the effect of isoprenaline on conduction velocity. This likely involves
296 receptor activation of M₂ muscarinic receptors coupled to inhibitory G-proteins that directly
297 antagonise the response at the level of adenylate cyclase (10). The G_{i2} isoform seems to be
298 central to muscarinic receptor signalling: L-type calcium channel modulation in ventricular
299 myocytes is known to be abolished in G_{i2} knockout mice (8). The slow conduction may be
300 pro-arrhythmic through promotion of re-entry and wavebreak. Importantly, the increases in
301 MID observed in *Scn5a*^{+/-} hearts provide evidence of the propensity for this group to have
302 greater induced (rather than fixed) conduction velocity slowing. The implication therefore is
303 that the consistency of conduction may become destabilised when challenged by premature
304 extrastimuli in the context of autonomic modulation; whilst in the steady-state or resting
305 condition these hearts exhibit conduction velocity dynamics similar to those in wild-type
306 littermates.

307 The marked differences in baseline conduction velocities between the tissue slice
308 preparations and the whole heart Langendorff preparations may result from the involved
309 tissue preparation techniques required to obtain viable slices. Even limited tissue disruptions
310 that may have occurred during slice preparation could lead to reductions in cell-to-cell
311 coupling, and thus accentuate pre-existing conduction delays.

312 In understanding the human Brugada syndrome two main hypotheses have been
313 advanced (3; 15; 22): either that conduction is slowed and thus activation delayed or that
314 repolarisation occurs prematurely. More specifically, coved ST segment elevation in ECG
315 leads V1-V3, often taken as the hallmark of the syndrome, equates to either delayed
316 depolarisation from the RV body to the RVOT or a shortened action potential in the
317 epicardium leading to repolarisation gradients across the right ventricular wall. The present

318 findings in this mouse model show that autonomic activation has the potential to significantly
319 modulate conduction delays, particularly in the context of pre-existing conduction deficiency.
320 Our major finding is that adrenergic increases in conduction velocity are impaired in the
321 *Scn5a*^{+/-} mouse. This process in the normal murine heart is antagonised by muscarinic
322 receptor activation but lost in the sodium channel haploinsufficient mouse. In the intact
323 animal there will be a degree of autonomic balance and even at rest vagal tone will be
324 modified by a degree of sympathetic drive. The absolute slowing may then be greatest when
325 high vagal tone is combined with cardiac sodium channel haploinsufficiency. We have
326 recently completed a study in man examining the effects of edrophonium on endocardial and
327 epicardial right ventricular electrophysiology (5). We demonstrated that edrophonium
328 appears to modulate both conduction and repolarisation in patients with BrS, particularly
329 delaying activation and repolarisation in the right ventricular epicardium, in line with these
330 presented results.

331 Though the use of isolated tissue from transgenic mice permits study of tissue-level
332 phenomena, this approach does have limitations which are reflected in this study. The
333 relatively small anatomy and thin ventricular walls did not permit detailed examination of
334 differential epicardial and endocardial characteristics or selective studies of the right
335 ventricular outflow tract. However with some adaptation of the array technology this may be
336 possible in the future. In a previous study, only a trend to an increase in conduction velocity
337 with isoprenaline was observed which did not reach statistical significance. (17). Variations
338 in animal lines may explain such variance. Sodium channel mutations leading to phenotypic
339 disease can occur in families where BrS is inherited in an autosomal dominant fashion. In
340 general these mutations lead to a loss of sodium channel function and the disease is generated
341 by *SCN5A* haploinsufficiency (13; 26). However in the majority of patients no mutation is
342 obvious, the disease occurs sporadically and may have a different pathogenesis (13; 26).

343 Caution must therefore be exercised in applying the results of animal studies to this human
344 syndrome.

345 In conclusion we have examined the influence of autonomic regulation on tissue level
346 cardiac electrophysiology in a mouse model of BrS. Haploinsufficiency of *Scn5a* leads to
347 impairment of conduction velocity reserve with blunting of sympathetically mediated
348 increases and reversal by muscarinic receptor activation compared to littermate control mice.

349

350 **Acknowledgements**

351 JBA was funded by a Heart Research UK Fellowship, MO is funded by a Marie Curie
352 Fellowship, DS funded by an MRC CASE Studentship, PDL is supported by UCLH
353 Biomedicine NIHR, Barts BRC & Stephen Lyness Memorial Fund & CLHH is funded by the
354 British Heart Foundation. AT is supported by the British Heart Foundation
355 (RG/15/15/31742). AT and MF were facilitated in this project by the NIHR Biomedical
356 Research Centre at Barts. The authors have no conflicts of interest.

357

358 **Figure Legends**

359

360 **Figure 1. Measurement of conduction velocity and Mean Increase in Delay from**
361 **multielectrode array. A.** An example electrogram from a single electrode of a multielectrode
362 array is shown. The local activation time is taken as the dV/dt min (arrow), during calculation
363 the pacing artefact is blanked. **B.** Each electrogram and activation time is assigned to a 2D
364 coordinate on a grid reflecting the geometry of the multielectrode array. Local activation time
365 is determined for all the electrodes on the grid. Electrode numbers are given as E1, E2 etc. **C.**
366 The gradient of activation times is then determined by interpolation (shown as a colourmap).
367 The inverse of this “activation time gradient” can be determined to give the conduction
368 velocity. The median conduction velocity over the multielectrode array was used for
369 measurement. **D.** Determination of Mean Increase in Delay. The activation time is plotted for
370 a series of S1S2 coupling intervals. The mean change in activation time over this interval (the
371 Mean Increase in Delay, MID) is calculated by determining the area of the activation time
372 change with coupling interval change (shaded area in figure). This area is divided by the
373 Change in Coupling Interval to give the unit Mean Increase in Delay. The MID allows the
374 susceptibility to conduction slowing with coupling interval changes to be compared.

375

376 **Figure 2. Murine tissue slice conduction velocity (CV) measurements.** A. Light
377 microscope image of ventricular slice section on multielectrode array. B. Example
378 electrograms acquired from WT and *Scn5a*^{+/-} mice hearts under baseline and isoprenaline
379 challenge. C. The effects of isoprenaline (Iso) and the ACh agonist carbachol (Carb) are
380 shown in the 2 murine groups. A significant increase in CV is seen in response to isoprenaline
381 which is absent in the *Scn5a*^{+/-} mice. This effect is abolished by carbachol. Asterisks indicate

382 statistical significances from comparisons between *Scn5a*^{+/-} and wild type (** p<0.01,
383 ***p<0.001).

384

385 **Figure 3. Electrophysiological properties of Langendorff-perfused hearts from *Scn5a*^{+/-}**
386 **and wild type mice under isoprenaline challenge.** A. Conduction velocity dynamics
387 mirrored those seen in tissue slice preparations, with paradoxical responses to isoprenaline
388 challenge in the heterozygous mouse hearts. The MID of *Scn5a*^{+/-} hearts was markedly
389 greater than those of WT animals (B). Unlike tissue slices, only marginal differences in ERP
390 were observed in whole heart preparations (C). Asterisks indicate statistical significances from
391 comparisons between *Scn5a*^{+/-} and wild type (** p<0.01, ***p<0.001).

392

393 **Figure 4. The localisation of Cx43 in *Scn5a*^{+/-} and wild type mice using laser scanning**
394 **confocal microscopy.** Representative heart sections are shown with N-cadherin staining
395 marking the intercalated disc and DAPI the nucleus. Cx43 is expressed and present at the
396 intercalated disc however there is an impression of mislocalisation of Cx43 away from the
397 intercalated disc. This is confirmed using a numerical approach as detailed in the text. The
398 sections are representative of a number of sections from a single mouse and the experiment
399 was repeated in an additional littermate control and *Scn5a*^{+/-} mouse (n=5 total sections in
400 each group).

401

402

403

404

405

406

407

408

409

410

411

412

413

414

415

416

417

418

419

420

421

422

423

Reference List

1. **Agullo-Pascual E, Lin X, Leo-Macias A, Zhang M, Liang FX, Li Z, Pfenniger A, Lubkemeier I, Keegan S, Fenyo D, Willecke K, Rothenberg E and Delmar M.** Super-resolution imaging reveals that loss of the C-terminus of connexin43 limits microtubule plus-end capture and NaV1.5 localization at the intercalated disc. *Cardiovasc Res* 104: 371-381, 2014.
2. **Ajjola OA, Lux RL, Khahera A, Kwon O, Aliotta E, Ennis DB, Fishbein MC, Ardell JL and Shivkumar K.** Sympathetic modulation of electrical activation in normal and infarcted myocardium: implications for arrhythmogenesis. *Am J Physiol Heart Circ Physiol* 312: H608-H621, 2017.
3. **Antzelevitch C.** Genetic, molecular and cellular mechanisms underlying the J wave syndromes. *Circ J* 76: 1054-1065, 2012.
4. **Bezzina CR, Lahrouchi N and Priori SG.** Genetics of sudden cardiac death. *Circ Res* 116: 1919-1936, 2015.
5. **Bhar-Amato J, Finlay M, Santos D, Orini M, Chaubey S, Vyas V, Taggart P, Grace AA, Huang CL, Ben SR, Tinker A and Lambiase PD.** Pharmacological Modulation of Right Ventricular Endocardial-Epicardial Gradients in Brugada Syndrome. *Circ Arrhythm Electrophysiol* 11: e006330, 2018.

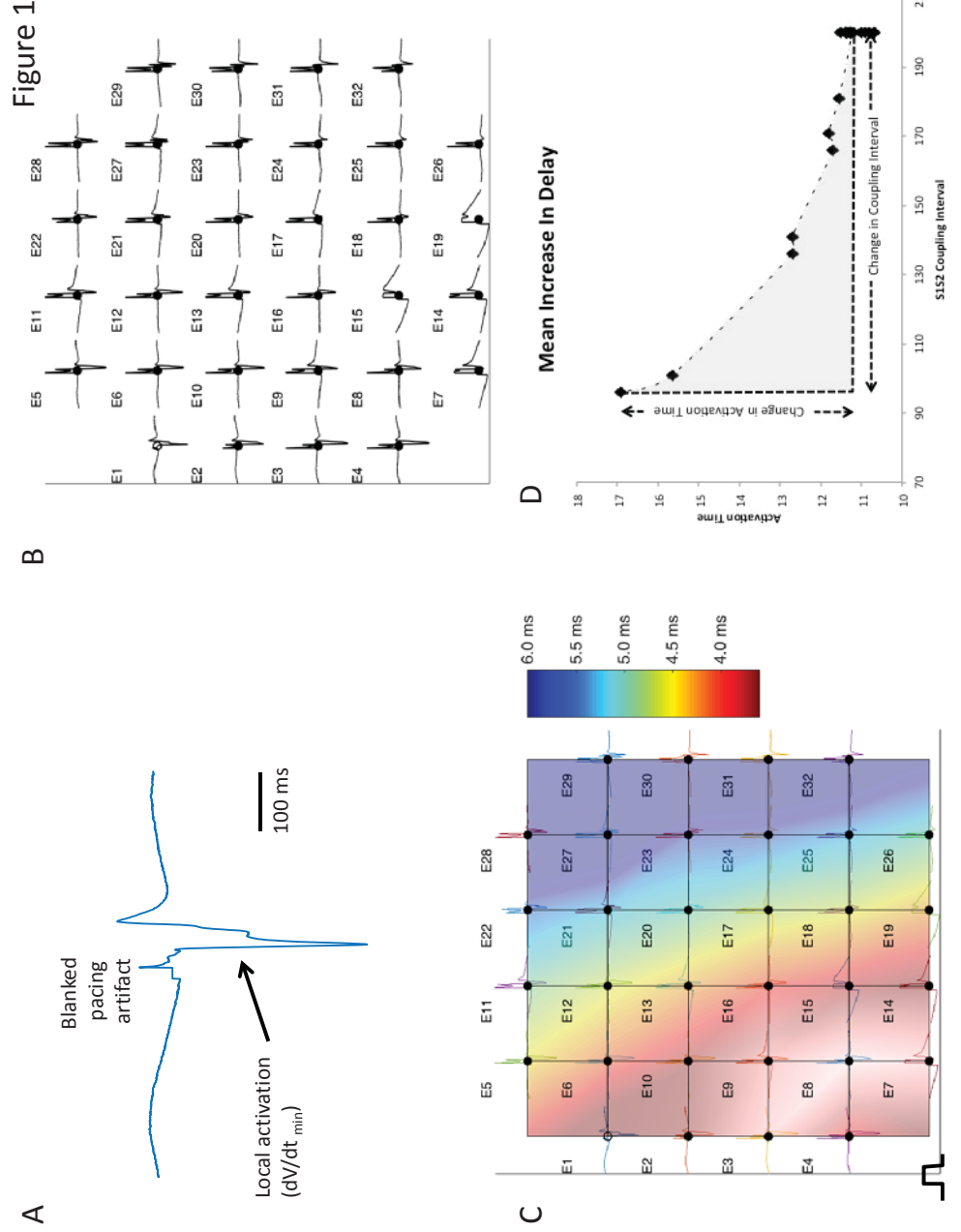
- 424 6. **Brugada P and Brugada J.** Right bundle branch block, persistent ST segment elevation
425 and sudden cardiac death: a distinct clinical and electrocardiographic syndrome. A
426 multicenter report. *J Am Coll Cardiol* 20: 1391-1396, 1992.
- 427 7. **Campbell AS, Johnstone SR, Baillie GS and Smith G.** beta-Adrenergic modulation of
428 myocardial conduction velocity: Connexins vs. sodium current. *J Mol Cell Cardiol* 77:
429 147-154, 2014.
- 430 8. **Chen F, Spicher K, Jiang M, Birnbaumer L and Wetzel GT.** Lack of muscarinic
431 regulation of Ca(2+) channels in G(i2)alpha gene knockout mouse hearts. *Am J Physiol*
432 *Heart Circ Physiol* 280: H1989-H1995, 2001.
- 433 9. **Finlay M, Harmer SC and Tinker A.** The control of cardiac ventricular excitability by
434 autonomic pathways. *Pharmacol Ther* 174: 97-111, 2017.
- 435 10. **Gomez J, Zhang L, Kostenis E, Felder CC, Bymaster FP, Brodtkin J, Shannon H,**
436 **Xia B, Duttaroy A, Deng CX and Wess J.** Generation and pharmacological analysis of
437 M2 and M4 muscarinic receptor knockout mice. *Life Sci* 68: 2457-2466, 2001.
- 438 11. **Jeevaratnam K, Guzadhur L, Goh YM, Grace AA and Huang CL.** Sodium channel
439 haploinsufficiency and structural change in ventricular arrhythmogenesis. *Acta Physiol*
440 *(Oxf)* 216: 186-202, 2016.
- 441 12. **Jeevaratnam K, Poh TS, Zhang Y, Rewbury R, Guzadhur L, Duehmke R, Grace**
442 **AA, Lei M and Huang CL.** Delayed conduction and its implications in murine

- 443 Scn5a(+/-) hearts: independent and interacting effects of genotype, age, and sex.
444 *Pflugers Arch* 461: 29-44, 2011.
- 445 13. **Kapplinger JD, Tester DJ, Alders M, Benito B, Berthet M, Brugada J, Brugada P,**
446 **Fressart V, Guerchicoff A, Harris-Kerr C, Kamakura S, Kyndt F, Koopmann TT,**
447 **Miyamoto Y, Pfeiffer R, Pollevick GD, Probst V, Zumhagen S, Vatta M, Towbin**
448 **JA, Shimizu W, Schulze-Bahr E, Antzelevitch C, Salisbury BA, Guicheney P, Wilde**
449 **AA, Brugada R, Schott JJ and Ackerman MJ.** An international compendium of
450 mutations in the SCN5A-encoded cardiac sodium channel in patients referred for
451 Brugada syndrome genetic testing. *Heart Rhythm* 7: 33-46, 2010.
- 452 14. **King JH, Huang CL and Fraser JA.** Determinants of myocardial conduction velocity:
453 implications for arrhythmogenesis. *Front Physiol* 4: 154, 2013.
- 454 15. **Lambiase PD, Ahmed AK, Ciaccio EJ, Brugada R, Lizotte E, Chaubey S, Ben-**
455 **Simon R, Chow AW, Lowe MD and McKenna WJ.** High-density substrate mapping
456 in Brugada syndrome: combined role of conduction and repolarization heterogeneities in
457 arrhythmogenesis. *Circulation* 120: 106-4, 2009.
- 458 16. **Lambiase PD and Tinker A.** Connexins in the heart. *Cell Tissue Res* 360: 675-684,
459 2015.
- 460 17. **Lane JD, Montaigne D and Tinker A.** Tissue-Level Cardiac Electrophysiology Studied
461 in Murine Myocardium Using a Microelectrode Array: Autonomic and Thermal
462 Modulation. *J Membr Biol* 250: 471-481, 2017.

- 463 18. **Machhada A, Trapp S, Marina N, Stephens RCM, Whittle J, Lythgoe MF,**
464 **Kasparov S, Ackland GL and Gourine AV.** Vagal determinants of exercise capacity.
465 *Nat Commun* 8: 15097, 2017.
- 466 19. **Martin CA, Siedlecka U, Kemmerich K, Lawrence J, Cartledge J, Guzadhur L,**
467 **Brice N, Grace AA, Schwiening C, Terracciano CM and Huang CL.** Reduced Na(+)
468 and higher K(+) channel expression and function contribute to right ventricular origin of
469 arrhythmias in *Scn5a*^{+/-} mice. *Open Biol* 2: 120072, 2012.
- 470 20. **Matsuda JJ, Lee H and Shibata EF.** Enhancement of rabbit cardiac sodium channels
471 by beta-adrenergic stimulation. *Circ Res* 70: 199-207, 1992.
- 472 21. **Matsuo K, Kurita T, Inagaki M, Kakishita M, Aihara N, Shimizu W, Taguchi A,**
473 **Suyama K, Kamakura S and Shimomura K.** The circadian pattern of the development
474 of ventricular fibrillation in patients with Brugada syndrome. *Eur Heart J* 20: 465-470,
475 1999.
- 476 22. **Meregalli PG, Wilde AA and Tan HL.** Pathophysiological mechanisms of Brugada
477 syndrome: depolarization disorder, repolarization disorder, or more? *Cardiovasc Res* 67:
478 367-378, 2005.
- 479 23. **Mizumaki K, Fujiki A, Tsuneda T, Sakabe M, Nishida K, Sugao M and Inoue H.**
480 Vagal activity modulates spontaneous augmentation of ST elevation in the daily life of
481 patients with Brugada syndrome. *J Cardiovasc Electrophysiol* 15: 667-673, 2004.

- 482 24. **Papadatos GA, Wallerstein PM, Head CE, Ratcliff R, Brady PA, Benndorf K,**
483 **Saumarez RC, Trezise AE, Huang CL, Vandenberg JI, Colledge WH and Grace**
484 **AA.** Slowed conduction and ventricular tachycardia after targeted disruption of the
485 cardiac sodium channel gene *Scn5a*. *Proc Natl Acad Sci U S A* 99: 6210-6215, 2002.
- 486 25. **Priori SG, Wilde AA, Horie M, Cho Y, Behr ER, Berul C, Blom N, Brugada J,**
487 **Chiang CE, Huikuri H, Kannankeril P, Krahn A, Leenhardt A, Moss A, Schwartz**
488 **PJ, Shimizu W, Tomaselli G, Tracy C, Ackerman M, Belhassen B, Estes NA, III,**
489 **Fatkin D, Kalman J, Kaufman E, Kirchhof P, Schulze-Bahr E, Wolpert C, Vohra J,**
490 **Refaat M, Etheridge SP, Campbell RM, Martin ET and Quek SC.** Executive
491 summary: HRS/EHRA/APHRS expert consensus statement on the diagnosis and
492 management of patients with inherited primary arrhythmia syndromes. *Europace* 15:
493 1389-1406, 2013.
- 494 26. **Sarquella-Brugada G, Campuzano O, Arbelo E, Brugada J and Brugada R.**
495 Brugada syndrome: clinical and genetic findings. *Genet Med* 18: 3-12, 2016.
- 496 27. **Shy D, Gillet L and Abriel H.** Cardiac sodium channel NaV1.5 distribution in
497 myocytes via interacting proteins: the multiple pool model. *Biochim Biophys Acta* 1833:
498 886-894, 2013.
- 499
500

Figure 1



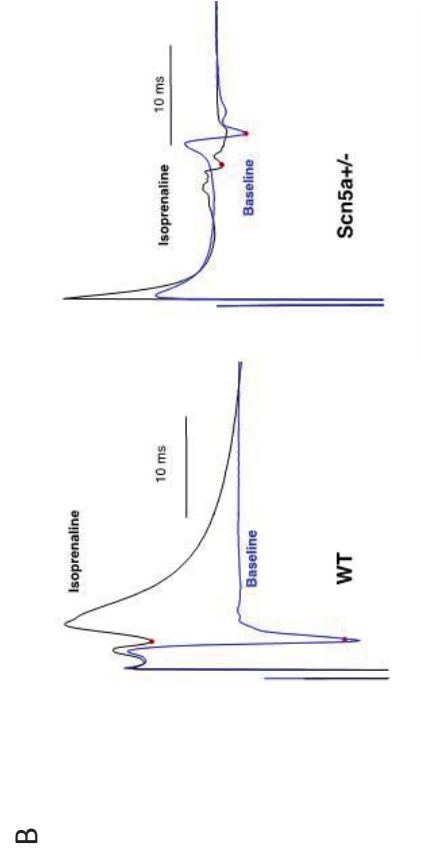
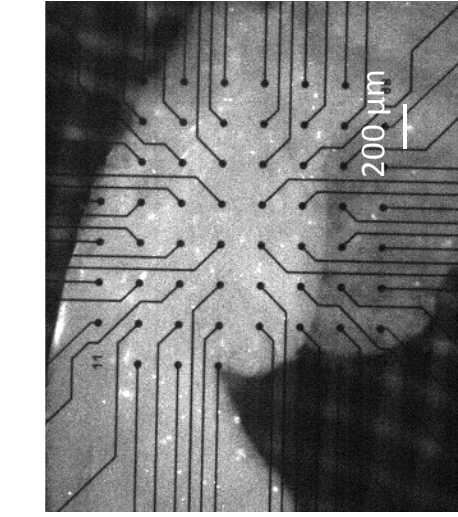
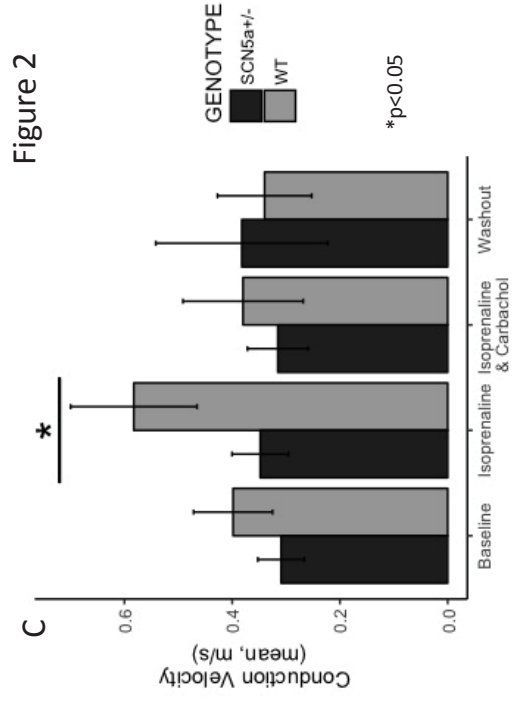
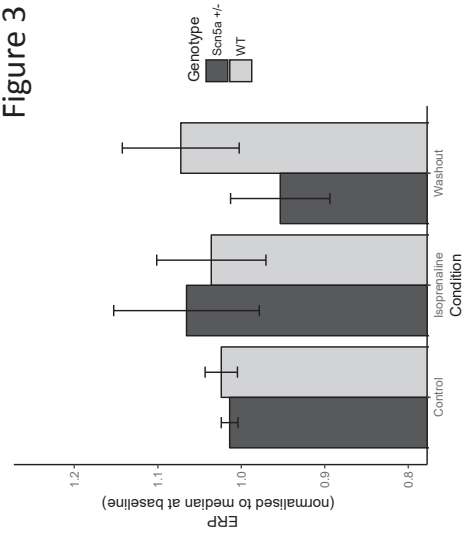
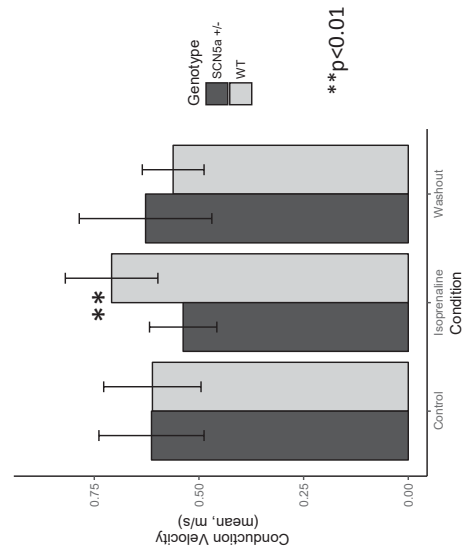


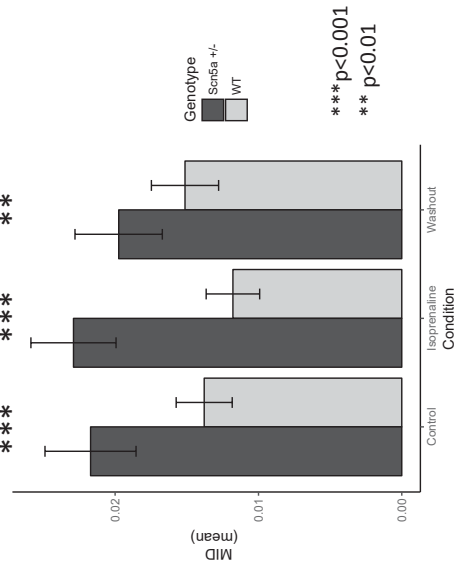
Figure 3



C



A



B

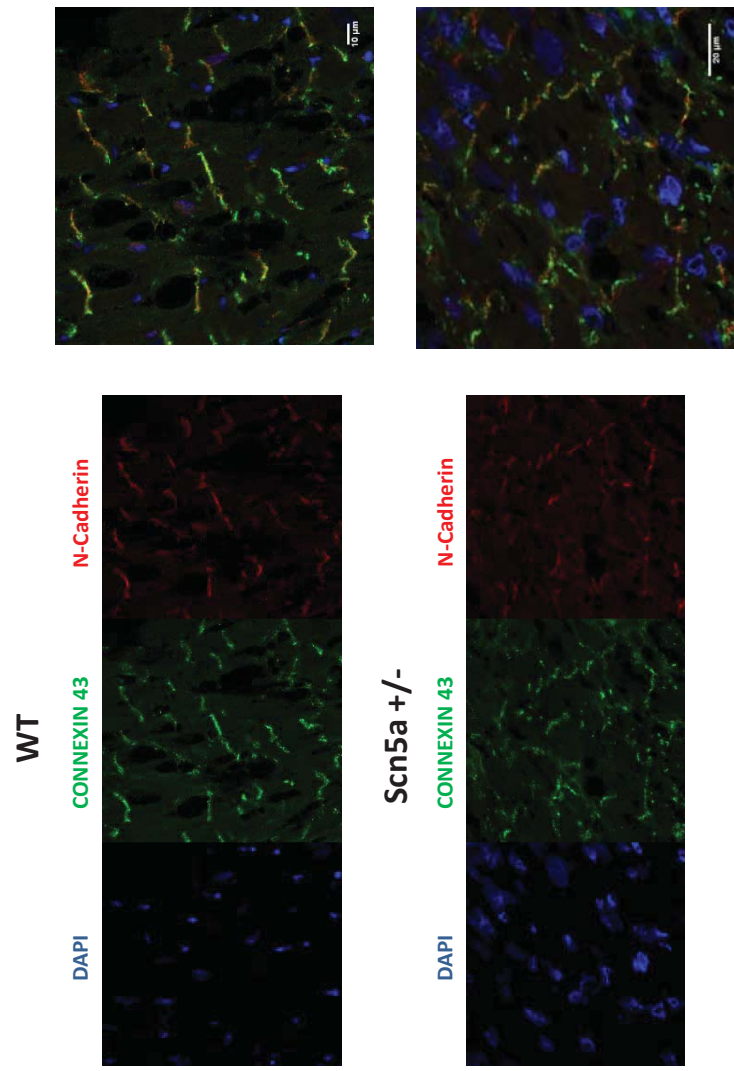


Figure 4